ACS APPLIED MATERIALS & INTERFACES

Research Article

Cite This: ACS Appl. Mater. Interfaces 2019, 11, 32613−32622

www.acsami.org

Porous Chitosan Films Support Stem Cells and Facilitate Sutureless Tissue Repair

Herleen Ruprai,[†] Sara Romanazzo,[⊥] Jake Ireland,[⊥] Kristopher Kilian,[⊥,#] Damia Mawad,[#,▽] Laurel George,[‡] Richard Wuhrer,[‡] Jessica Houang,[○] Daniel Ta,[†] Simon Myers,[†,§] and Antonio Lauto*[,†,§,∥]

[†]School of Science and Health, [‡]Advanced Materials Characterization Facility, [§]School of Medicine, and [∥]Biomedical Engineering & Neuroscience Research Group, The MARCS Institute, Western Sydney University, Locked Bag 1797, Penrith, NSW 2751, Australia

[⊥]School of Chemistry, [#]School of Materials Science and Engineering, and [▽]Australian Centre for NanoMedicine and ARC Centre of Excellence in Convergent BioNano Science and Technology, and Centre for Advanced Macromolecular Design, University of New South Wales, Sydney, NSW 2052, Australia

[○]Biomedical Engineering, School of Aerospace, Mechanical and Mechatronic Engineering, University of Sydney, Sydney, NSW 2006, Australia

Supporting Information

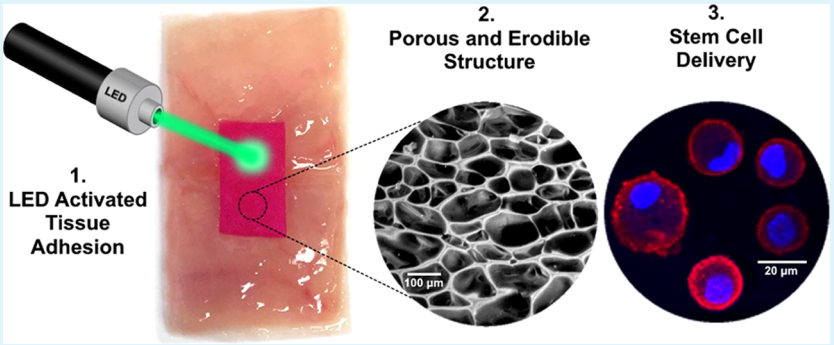

ABSTRACT: Photochemical tissue bonding with chitosan-based adhesive films is an experimental surgical technique that avoids the risk of thermal tissue injuries and the use of sutures to maintain strong tissue connection. This technique is advantageous over other tissue repair methods as it is minimally invasive and does not require mixing of multiple components before or during application. To expand the capability of the film to beyond just a tissue bonding device and promote tissue regeneration, in this study, we designed bioadhesive films that could also support stem cells. The films were modified with oligomeric chitosan to tune their erodibility and made porous through freeze-drying for better tissue integration. Of note, porous adhesive films (pore diameter ∼110 μm), with 10% of the chitosan being oligomeric, could retain similar tissue bonding strengths (13−15 kPa) to that of the nonporous chitosan-based adhesives used in previous studies when photoactivated. When tested in vitro, these films exhibited a mass loss of ∼20% after 7 days, swelling ratios of ∼270−300%, a percentage elongation of ∼90%, and both a tensile strength and Young's modulus of ∼1 MPa. The physical properties of the films were suitable for maintaining the viability and multipotency of bone-marrow-derived human mesenchymal stem cells over the duration of culture. Thus, these biocompatible, photoactivated porous, and erodible adhesive films show promise for applications in controlled cell delivery and regenerative medicine.

KEYWORDS: *adhesive biomaterials, photochemical bonding, regenerative medicine, lasers, LED*

1. INTRODUCTION

Photochemical tissue bonding (PTB) is an alternative surgical technique that involves the use of light energy and photosensitizers to bond tissue edges or surfaces together through nonthermal mechanisms. PTB is commonly mediated through green light and photoactive dyes such as rose bengal, which when photoactivated, facilitate amino acid crosslinking reactions mainly through the production of singlet oxygen.[1] This repair method has shown to be valuable in a variety of surgical procedures involving the skin,[2] eye,[3] blood vessels,[4] and vocal cords.[5] However, using the dye alone with green light often does not provide enough mechanical strength in some procedures without extra support from grafts or sutures.[6,7] This disadvantage is also shared with many of the commercially available tissue adhesives, which have poor mechanical properties under high tensile loads.[8] Similarly,

Received: May 25, 2019
Accepted: August 16, 2019
Published: August 16, 2019

DOI: 10.1021/acsami.9b09123
ACS Appl. Mater. Interfaces 2019, 11, 32613−32622

sutures have their limitations including postoperative complications such as tissue trauma, inflammation, and scarring,[2,9,10] and the requirement for great dexterity as using a needle and thread on small anatomical structures is difficult.

Several studies have demonstrated that a strong sutureless support can be provided by PTB through chitosan films loaded with rose bengal.[9,11,12] These adhesive films have the advantage of being biocompatible,[9,13] biodegradable (can be broken down by lysozymes),[14] easy to use (films are simply applied on the tissue and illuminated with green light),[15] robust (in vivo, they could support the reconnection of nerves and withstand the forces of a beating heart),[10,11,16] nonthermal (tissue temperature remained below 40 °C during irradiation),[17] and controllable (the bonding strength can be adjusted by the irradiation parameters).[18] Yet, their capability to promote tissue regeneration is limited by their nonporous and slowly degrading structure.

In this study, we developed porous chitosan-based adhesive films through freeze-drying to optimize cell growth and proliferation when soft tissue wound edges are approximated. Freeze-drying is a low-temperature and low-vacuum dehydration process. It is a well-established technique in industry and commonly used for fabricating interconnected porous materials that can mimic the porous structure of extracellular matrices (ECMs) in the body.[19] Materials that mimic aspects of the native ECM are useful as implantable biomaterials for tissue regeneration because they can be designed to support survival, growth, and differentiation and secretory profiles that promote healing. In particular, implanting biomaterials with stem cells can be used to reduce scar formation of tissues that are unable to self-regenerate.[20] Here, we explored the integration of human mesenchymal stem cells (hMSCs) with our chitosan materials. hMSCs have the propensity to differentiate into numerous lineages and have demonstrated therapeutic efficacy in treating cardiovascular diseases through trophic and immunomodulatory activities.[21−23]

To make the adhesive films more degradable, without adding expensive additives such as degradative enzymes or using multistep conjugation procedures, films with a blend of medium-molecular-weight (MW) and oligomeric chitosan (water-soluble chitosan) were tested. Generally, polymers based on a blend of medium- and low-molecular-weight polymers tend to be more soluble in water than those based purely on medium-weight polymers.[24] The addition of oligomeric chitosan was hypothesized as a way to simply tune the erosion rate of the films for different cell delivery applications.

The efficacy of this design approach was evaluated by comparing the differences in the mechanical, swelling, erosion, and adhesive properties between films with and without pores and oligomeric chitosan. Those films that displayed ideal properties, i.e., were able to erode over time under physiological conditions, had pores for cell and nutrient exchange, and had similar adhesion properties to our previous robust nonporous insoluble adhesive films, were then tested in vitro with hMSCs. The aim of this study was to obtain a bioadhesive film that can adhere to soft tissue without sutures and at the same time support soft tissue regeneration.

2. MATERIALS AND METHODS

2.1. Materials. Oligomeric chitosan was purchased from AK Biotech Ltd. (Jinan, China). All other chemicals in Sections 2.2−2.8 were obtained from Sigma-Aldrich (Sydney, Australia) and used as received. Reagents used for the in vitro stem cell study (Section 2.9) were purchased from ThermoFisher Scientific (Melbourne, Australia) or an alternate source otherwise stated.

Sheep small intestine sections (20 cm) were collected immediately after sheep euthanasia (Wollondilly Abattoir Pty Ltd.), flushed with room-temperature (∼25 °C) water, and stored at −80 °C within 1−2 h after animal sacrifice. Before being used for experiments, the intestine sections were defrosted and washed thoroughly with room-temperature water. Mesenteric tissues on the intestine sections were also removed.

Bone-marrow-derived hMSCs were purchased from Lonza, cultured, and expanded in fully supplemented mesenchymal stem cell basal medium (Lonza) according to the manufacturer's instructions. Cells were then cryopreserved in 10% dimethyl sulfoxide solution at passage 2, thawed, and cultured in the so-called complete medium, containing Dulbecco's modified Eagle's medium and low glucose (1000 mg L^{-1}) (Invitrogen) media supplemented with 10% fetal bovine serum (Bovogen) and 1% penicillin/streptomycin (Invitrogen). The medium was changed every 3 days, and cells were passaged at 70% confluency using a solution containing 0.025% trypsin/1 mM. Cells were then used for experiments between passage 5 and 8.

2.2. Adhesive Film Preparation. The films were made from solutions listed in Table 1 and prepared using the protocol previously described by Lauto and co-workers.[15] Two blends of oligomeric chitosan (MW ∼ 5 kDa, ∼80% deacetylated) and medium-molecular-weight chitosan (MW ∼ 250 kDa, ∼80% deacetylated) were prepared and compared to the standard composition used in previous reports.[15,17] The protocol involved mixing chitosan, rose bengal, and acetic acid together into deionized water for 2 weeks at room temperature (∼25 °C) under a dark cover, removing undissolved matter by centrifugation (1 h, 3270*g*, 25 °C), and storing the decanted supernatant at 4 °C until further use.

Table 1. Solutions Used To Fabricate the Adhesive Films[a]

solution	medium-MW chitosan (% w/v)	oligomeric chitosan (% w/v)	acetic acid (% v/v)	rose bengal (% w/v)
standard	1.70	0	2	0.01
oligomeric 10%	1.53	0.17	2	0.01
oligomeric 30%	1.19	0.51	2	0.01

[a]The label "oligomeric" signifies the percentage of chitosan that is oligomeric chitosan in the composition; in the standard composition, there is no oligomeric chitosan; in the oligomeric 10% composition, 10% of the chitosan is oligomeric; and in the oligomeric 30% composition, 30% of the chitosan is oligomeric. The standard solution is the composition used in previous studies.[15,17] Components were dissolved in deionized water.

To fabricate porous adhesive films, 3 mL of prepared solutions was pipetted into plastic Petri dishes (3 × 4 cm^2), frozen (24 h, −30 °C), and then freeze-dried (6 h, −50 °C, 0.1 mbar). The films were further air-dried for 3 weeks at room temperature under a dark cover to reduce their moisture content. The dried films were carefully detached from the Petri dishes using a spatula and cut into the desired dimensions for testing. These pieces were stored between clean glass slides to maintain a flattened geometry and wrapped with parafilm and aluminum foil at room temperature to avoid photobleaching of rose bengal until further use. The thickness of the flattened porous films was within 340−370 μm when measured at five different points with a digital micrometer (model 293-831, Mitutoyo, Japan). Nonporous films were also fabricated for comparison and prepared in the same way except that the solution (2.3 mL) was only air-dried at room temperature for 3 weeks under a dark cover and not frozen nor lyophilized. The thickness of the nonporous films ranged between 20 and 25 μm.

DOI: 10.1021/acsami.9b09123
ACS Appl. Mater. Interfaces 2019, 11, 32613−32622

2.3. Tissue Adhesion Measurement. The tissue bonding properties of the films were assessed on sheep small intestine tissue ex vitro using a procedure similar to that used in a previous study.[17] Sheep small intestine was selected for three reasons: (1) its serosa layer contains collagen, a protein found on many soft tissues in the body, (2) one whole small intestine can supply for several tests, and (3) it can be easily cut into many pieces. For the measurements, a tissue piece (1.5 × 4 cm^2) was dipped into water at room temperature (~25 °C) and bisected with scissors. The tissue ends were approximated together with microforceps under an operating microscope (magnification 20×). Excess water on the tissue was removed with cotton tips, and the adhesive film (1.0 × 0.6 cm^2) was positioned over the bisection line on the serosa layer of the tissue. The film was then spot-irradiated with a continuous wave of green light-emitting diode (LED) light (515 nm) (Ultra High-Power Microscope LED, Prizmatix), which was coupled to an optical fiber with a core diameter of 200 μm. A fluence of 110 J cm^{-2} was delivered over the area of the film by scanning the green light beam across the film multiple times in ~0.5 cm diameter spots at an intensity of 180 mW for 5 s before moving to an adjacent spot (irradiance ~0.9 W cm^{-2}). The total irradiation time was ~6 min. The repaired moist tissue sample (maintained in a wet gauze to avoid tissue desiccation) was then clamped into a calibrated single-column tensiometer (Instron 3343, Instron), which moved at a rate of 22 mm min^{-1}. The maximum force required to separate the repaired tissue was recorded, and the tissue bonding strength was estimated by dividing the maximum force by the area of the film. The area under the tensiometer force versus extension curve was also measured and defined as the tissue adhesion energy of the films; this parameter was calculated with tensiometer software (Instron, Bluehill 2). Thirty samples from each group were tested. Tissues repaired with films without LED irradiation were also tested for comparison.

2.4. Atomic Force Spectroscopy. An atomic force microscope (AFM) (NanoWizard II, JPK Instruments, Germany) was used to further analyze the adhesion properties and toughness of the films. Force spectroscopy measurements were performed with silicon cantilever tips (spring constant, 0.3 N m^{-1}; resonant frequency, 14–17 kHz; SICON, AppNano); the cantilevers were independently calibrated with the thermal noise method embedded in AFM software prior to use. To secure the films in the AFM, the films (1 × 1 cm^2) were attached onto the bottom of small plastic Petri dishes (3.5 cm diameter) with a very thin layer of epoxy (Loctite). Deionized water (~25 °C, 2 mL) was then injected into the Petri dishes to minimize capillary effects and eliminate the electrical charges accumulated on the sample surface. Consequently, the pull-off force measured in water represents the adhesive effect caused mostly by the van der Waals interaction between the sample and tip.[25] The following AFM parameters were held constant: 2.0 μm *Z*-length, 2.0 s extend time, and a relative set point of 5 nN. Force versus extension profiles were recorded between the AFM tip and sample surface in nine different locations over the sample area (50 × 50 μm^2) for six films from each group (n = 54). The energy required to detach the AFM tip from the sample surface was calculated as the area under the force versus extension curve and was recorded as the AFM tip adhesion energy; this parameter was calculated with JPK data processing software.

2.5. Erosion Study. Film solubility was measured in phosphate-buffered saline (PBS) at 37 °C to mimic in vivo conditions. Each film (2 × 2 cm^2) was placed into 50 mL of PBS (pH = 7.4) for 1 week and incubated in a constant-temperature water bath set at 37 °C; fresh PBS was replaced daily. At different time points, the film was removed from the PBS, lyophilized, and reweighed (m_d). The film was lyophilized prior to testing to obtain the initial mass of the film (m_i). Six samples were tested from each group. The percentage mass loss of the film in PBS at each time point was calculated using eq 1

$$\% \text{ mass loss} = \frac{m_i - m_d}{m_i} \times 100 \quad (1)$$

2.6. Swelling Study. The films were suspended in PBS at 37 °C to examine their swelling behavior in conditions similar to an in vivo environment. Before immersion in PBS, the initial mass (m_i) of each film (2 × 2 cm^2) was measured. Each film was then placed in 50 mL of PBS (pH = 7.4) and incubated in a constant-temperature water bath set at 37 °C. At different time points, the film was removed from the PBS, gently dry-blotted with a Kim Wipe, and reweighed (m_s). Six films from each group were tested. The percentage mass swelling ratio of the film at each time point was calculated using eq 2

$$\% \text{ swelling ratio} = \frac{m_s - m_i}{m_i} \times 100 \quad (2)$$

2.7. Mechanical Test. The tensile strength, percentage elongation, and Young's modulus of the films were determined with the 3343 Instron tensiometer (Instron). The film (0.6 × 3.0 cm^2) was dipped into PBS for 10 s at room temperature (~25 °C) to mimic the wet conditions when used on moist tissue. The film was then clamped to the tensiometer (grip gap = 1 cm), which was set to a loading rate of 22 mm min^{-1} until the film ruptured cohesively (broke into two pieces). The tensile strength was calculated as the maximum load force divided by the width and thickness of the film (width and thickness were assumed constant during the test). Percentage elongation was calculated by dividing the maximum elongation of the film with the film's original length and multiplying this ratio by 100. Young's modulus was defined as the tangent slope at the linear portion of the tensiometer stress versus strain profile. These parameters were calculated with tensiometer software (Instron, Bluehill 2). Ten samples were measured from each group.

2.8. Scanning Electron Microscopy. A JEOL 6510 low-vacuum, scanning electron microscope (SEM) was used to observe the pore shape in the films and the adhesive–tissue interface. All samples were attached to aluminum stubs with double-sided conductive carbon tape. Images were collected with a backscatter detector, with the SEM operating under low vacuum at a pressure of 30 Pa, accelerating voltage of 15 kV, and a working distance of approximately 12 mm. For better visibility of the pores, the films (0.5 × 0.5 cm^2) were imaged "as is" and left unflattened after fabrication. Images taken at a magnification of 50× were used to measure the pore diameter in films. The pore diameter was defined as the square root of the product of the longest diameter and shortest diameter of the pore, since the pores in the films were not perfectly circular. The pore diameters were gauged in six different films (50 pores per film) for each group using the Aperio ImageScope program. To image the adhesive–tissue interface with the SEM, transverse sections (0.5 × 0.3 cm^2) of the intestine tissue photochemically bonded to the adhesive were cut and immediately fixed in Karnovsky's solution (2% v/v glutaraldehyde and 2.5% w/v paraformaldehyde in 0.1 M PBS) at 4 °C. After 24 h, the samples were rinsed with PBS for 15 min and dehydrated with a graded series of ethanol at concentrations of 30, 50, and 70% v/v.

2.9. In Vitro Stem Cell Study. *2.9.1. Cell Seeding.* The hMSCs were seeded on selected porous films. For this experiment, these films were fabricated without rose bengal as it absorbs in the same regions (500–600 nm) as the staining reagents used in confocal microscope imaging. These films were fabricated as outlined in Section 2.2 except that the solutions were mixed for a shorter period of 1 week (prolonged stirring is required with rose bengal due to its poor solubility in acidic solutions). The films were also sterilized with ethylene oxide before the test.

The films (1 × 1 cm^2) were placed into 12-well plates (Corning) and then soaked in Dulbecco's phosphate-buffered saline (DPBS) 1× for hydration. DPBS was then removed, and 1 mL of complete medium was added to each well. Samples were incubated at 37 °C and in a 5% CO_2 atmosphere for 30 min to 1 h. Meanwhile, hMSCs were trypsinized, centrifuged, and resuspended at a concentration of 3 × 10^4 cells in 50 μL volume. Cells were subsequently seeded onto the films by adding the 50 μL hMSC suspension on each sample and incubated in a 5% CO_2 atmosphere at 37 °C for 30 min; then, 1 mL of complete medium was added to each well and kept in culture for a period of 7 days.

2.9.2. Cell Viability Assay and Confocal Microscopy. Cell viability was established using a live/dead assay kit (Invitrogen). All samples were rinsed in DPBS and incubated for 1 h at 37 °C in a solution containing 2 μM calcein, for green staining of live cells, and 4 μM

DOI: 10.1021/acsami.9b09123
ACS Appl. Mater. Interfaces 2019, 11, 32613–32622

ethidium homodimer-1, a red label for dead cells. Following this, samples were rinsed again and imaged with the Nikon A1 confocal microscope at 488 and 543 nm wavelengths. Cell viability was then quantified using Image-J software.

2.9.3. Immunofluorescence Staining. For immunofluorescence studies, all samples were washed in DPBS and then fixed with 1% paraformaldehyde (Univar) at room temperature for 30 min. Following this, incubation with 0.1% Triton X-100 for 30 min was performed for cell membrane permeabilization. To analyze how cells were interacting with the films and if their morphology was influenced by this interaction, samples were incubated with tetra-rhodamine-conjugated phalloidin, a probe with high affinity for F-actin diluted in 1% bovine serum albumin (1:100; Invitrogen) for 1 h at room temperature. Nuclei were counterstained with 4′,6-diamidino-2-phenylindole (DAPI) (Sigma-Aldrich). To prove that the stem cells were able to maintain their undifferentiated state, samples were stained for h-Stro1 (1:200) and endoglin (1:100), by incubating them for 1 h at room temperature, and then the appropriate secondary antibodies, anti-mouse 488 (1:200) and anti-rabbit 546 (1:200) in 2% goat serum (Gibco), were used. Images were taken using the Nikon A1 confocal microscope at 488m, 546, and 358 nm. The confocal settings were as follows: pinhole, 26.82 airy unit; scan speed, 512 Hz unidirectional; and format, 1024 × 1024 pixels. Images were collected using the following laser wavelength settings: DAPI using 405 nm, STRO-1 using 488 nm, and endoglin using 640 nm.

2.10. Statistics. Data values were analyzed using paired *t*-tests or one-way analysis of variance (ANOVA) with Tukey's post-tests. Means were considered significantly different if $p < 0.05$. Values are expressed as mean ± standard deviation, and "*n*" represents the number of samples tested for a group.

3. RESULTS AND DISCUSSION

3.1. Porous Structure. The porous films were generated through freeze-drying, a process where the material is frozen, followed by sublimation of its ice crystals under low pressure to leave voids in the material. Porous structures promote healing as they provide an optimal microenvironment for the exchange of nutrients and wastes through the pores. When the chitosan-based solutions were frozen at −30 °C for 24 h and then sublimated, films with interconnected micropores were produced (Figure 1). The films made with the standard and oligomeric 10% compositions had similar pore diameters of 113 ± 26 and 110 ± 24 μm, respectively ($n = 300$, $p > 0.05$, one-way ANOVA Tukey's post-test). Conversely, films with oligomeric chitosan at 30% had smaller pore diameters of 52 ± 18 μm ($n = 300$, p values < 0.0001, one-way ANOVA Tukey's post-test), in agreement with the literature.[26]

3.2. Erodibility. It is important for the adhesive films to have appropriate degradation capabilities to enable the replacement of adhesive material with the host's extracellular matrix, avoid scar tissue encapsulation, and promote engraftment of implanted cells. The experimental results demonstrated that addition of biocompatible oligomeric chitosan was successful for increasing the erodibility of the adhesives in vitro. Within 1 week of incubation in PBS, the oligomeric 30% films exhibited the highest percentage mass loss (day 7 = 55−60% loss) followed by the oligomeric 10% films (day 7 = 15−20% loss) and the films made with the standard composition (day 7 = 4−6% loss) (Figure 2A). The higher erodibility of the oligomeric films is expected since oligomeric (low MW) chitosan is more soluble in water than medium-MW chitosan.[27] It should be also noted that a previous study established that irradiation does not affect the degradability of films based on chitosan and rose bengal.[14]

The porous films trended toward higher erosion rates than the nonporous films as shown in Figure 2A; however, there was no significant difference between the porous and nonporous films made from the standard composition at each time point ($p > 0.05$, one-way ANOVA, Tukey's post-test). The percentage mass loss for each film on each time point was also significantly different ($p < 0.0001$, one-way ANOVA). Images of the porous and nonporous films before and after immersion in PBS for 1 week at 37 °C are shown in Figure S1.

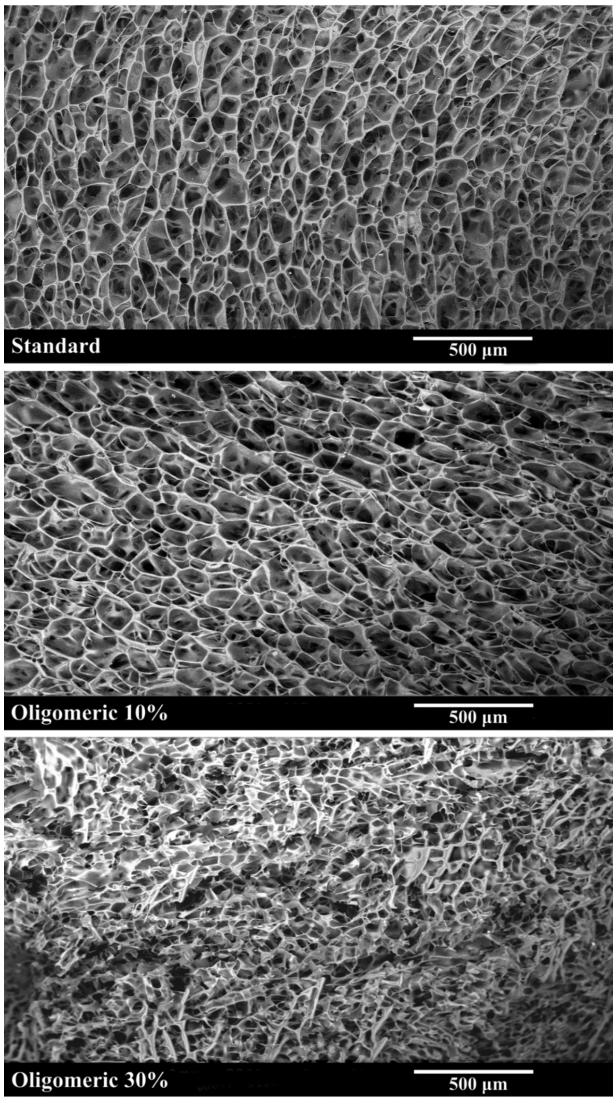

Figure 1. SEM images showing the surface of the standard, oligomeric 10%, and oligomeric 30% porous adhesive films. The oligomeric 30% films have smaller interconnected pores (pore diameter ∼50 μm) than the standard and oligomeric 10% films (pore diameters ∼110 μm).

3.3. Swelling. The mass swelling ratios of all films stabilized during the 30−120 min interval of incubation in PBS (Figure 2B). The porous films exhibited 2−3 times higher percentage mass swelling ratios than the nonporous adhesive films (220−320 vs 95−110%). These results confirm that the porous films are more permeable to their environment. The increased swelling of the porous films can be explained by their higher water absorbing ability via the capillary effects of the pores in the films. Films with oligomeric chitosan also trended toward lower percentage mass swelling ratios than films with the standard composition (Figure 2B). The lower swelling may be attributed to the mass loss of the films, especially for the porous oligomeric 30% films, which are highly erodible in PBS

DOI: 10.1021/acsami.9b09123
ACS Appl. Mater. Interfaces 2019, 11, 32613−32622

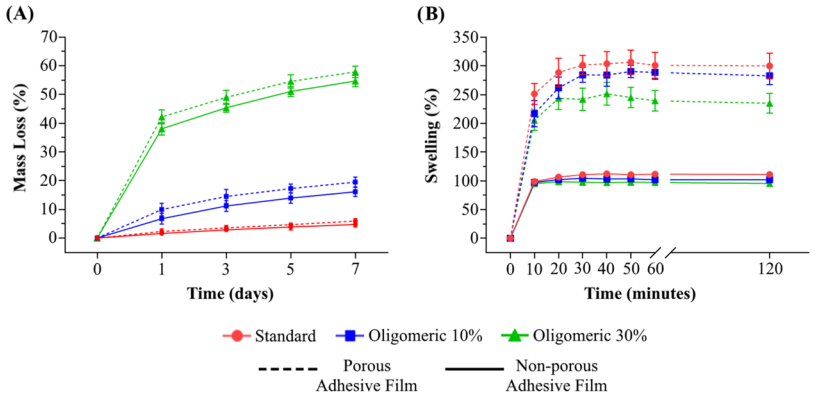

Figure 2. Percentage mass loss (A) and percentage mass swelling ratio (B) of porous and nonporous standard, oligomeric 10%, and oligomeric 30% adhesive films in PBS at 37 °C. Each point represents mean ± standard deviation (n = 6). Films with oligomeric chitosan were more soluble than the films made from the standard composition at each time point (p < 0.0001, one-way ANOVA, Tukey's post-test). Porous oligomeric films were also more soluble than nonporous ones at each time point (p < 0.05, one-way ANOVA, Tukey's post-test). The porous films significantly swelled more than the nonporous films at each time point (p < 0.0001, one-way ANOVA, Tukey's post-test). Within the porous and nonporous groups, films with oligomeric chitosan tended to have lower swelling ratios than films made from the standard composition; significant differences were detected between the standard films and oligomeric 30% films at each time point after 20 min (p < 0.05, one-way ANOVA, Tukey's post-test).

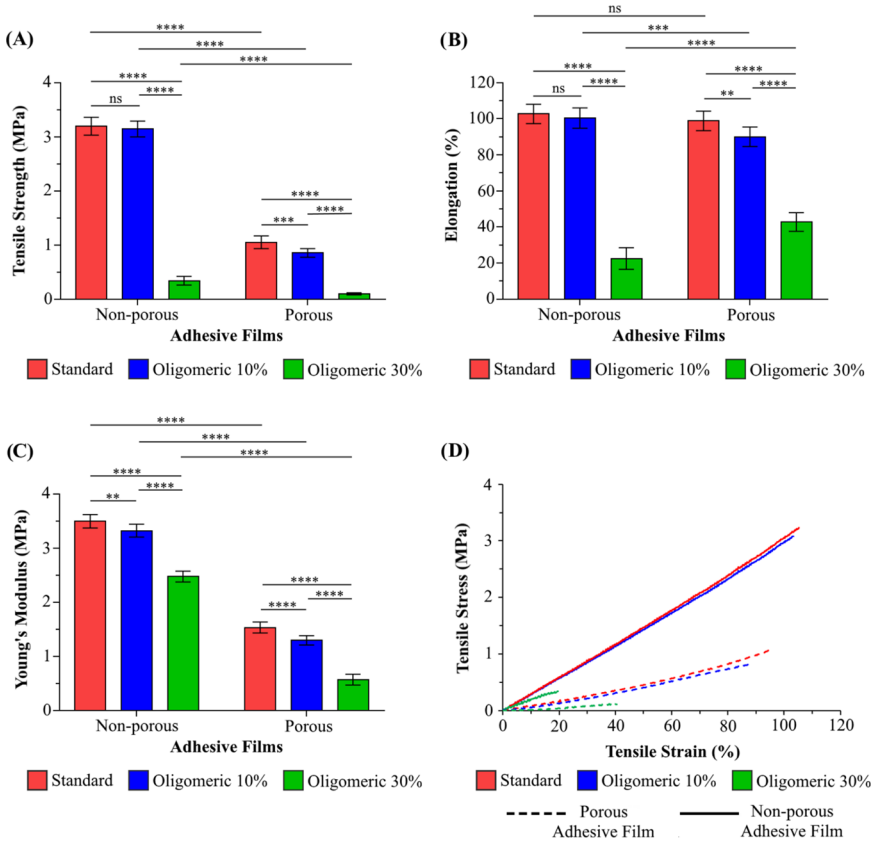

Figure 3. Tensile strengths (A), percentage elongations (B), Young's moduli (C), and representative stress vs strain profiles (D) of nonporous and porous standard, oligomeric 10%, and oligomeric 30% adhesive films. The films were wet when tested to mimic in vivo conditions. Porous films have lower tensile strengths and Young's moduli than nonporous films. In both porous and nonporous groups, the oligomeric 30% films had much lower tensile strengths, percentage elongations, and Young's moduli than standard films and oligomeric 10% films. Data represents mean ± standard deviation (n = 10). The symbol **** signifies p < 0.0001, *** signifies p < 0.001, ** signifies p < 0.01, and ns signifies p > 0.05 (p values determined by one-way ANOVA, Tukey's post-test).

(Figure 2A). Another study also found decreased swelling ratios for porous chitosan materials with greater solubility.[28]

3.4. Mechanical Properties. The mechanical properties of the films were tested to see whether the porous structure and addition of oligomeric chitosan changed the stiffness of the films; irradiation on the film has been previously shown to have no effect on the film's mechanical properties.[29] The films were also tested in a hydrated state to mimic the wet conditions inside the body. The tensile strength and Young's moduli of the porous films were approximately 20−40% of the nonporous films with the same compositions (p < 0.0001, one-way ANOVA, Tukey's post-test). The percentage

DOI: 10.1021/acsami.9b09123
ACS Appl. Mater. Interfaces 2019, 11, 32613−32622

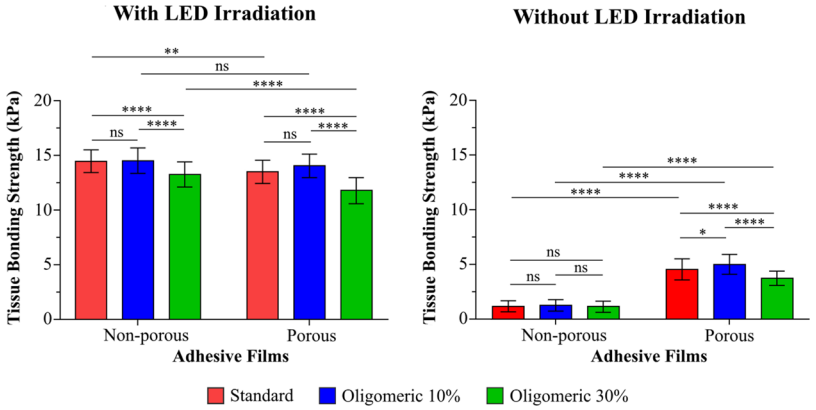

Figure 4. Tensile tissue bonding strengths of porous and nonporous standard, oligomeric 10%, and oligomeric 30% adhesive films with LED irradiation and without LED irradiation on sheep small intestine tissue. With irradiation, the nonporous and porous adhesives have bonding strengths that are within the range of each other. The effect of porosity and oligomeric chitosan on the tissue bonding strength for the adhesives with LED irradiation was small; some groups were found to be significantly different due to the large sample sizes used in the statistical test (n = 30). Without irradiation, the tissue bonding strength of the porous adhesives was greater than that of the nonporous adhesives; the addition of oligomeric chitosan did not heavily influence the tissue bonding strength in both groups despite some groups showing significant differences. The oligomeric 30% adhesives failed cohesively in all tests. The irradiated porous oligomeric 10% adhesives detached from the tissue interface in 80% of the tests (20% of the tests were due to cohesive failure). In every test for all other groups, tissue separation occurred at the tissue interface. Data represents mean ± standard deviation (n = 30). p values were determined by one-way ANOVA, Tukey's post-test, where **** signifies $p < 0.0001$, ** signifies $p < 0.01$, * signifies $p < 0.05$, and ns signifies $p > 0.05$.

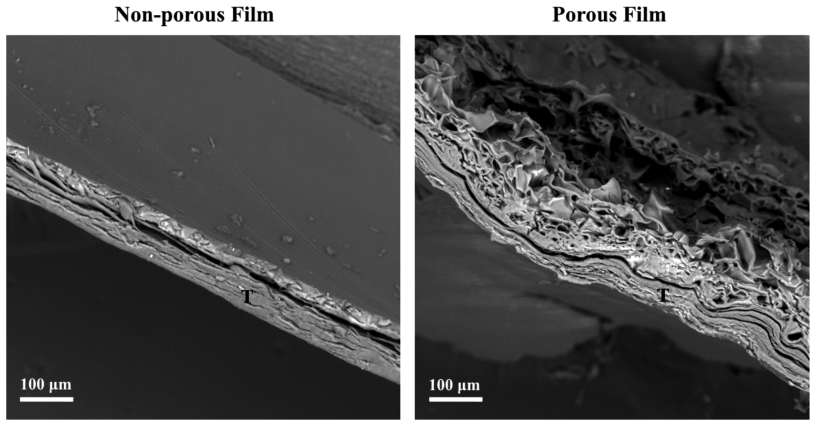

Figure 5. Cross-sectional SEM image of a nonporous film (standard) and a porous film (oligomeric 10%) photochemically bonded to sheep intestine tissue (T). The porous film can be seen to conform to tissue that closely follows the pore profile.

elongation for the porous and nonporous films with the same composition tended to be within the range of each other (Figure 3B). The lower stiffness of the porous film makes them more compatible for soft tissue integration.[30]

The addition of oligomeric chitosan at 30% greatly reduced the film's tensile strength, percentage elongation, and Young's modulus when compared to the standard and oligomeric 10% compositions ($p < 0.0001$, one-way ANOVA, Tukey's post-test). A composition of 10% oligomeric chitosan, however, did not significantly lower the mechanical properties of the films when compared to the standard composition (Figure 3). The results show that the stiffness of the adhesive films can be adjusted with the addition of oligomeric chitosan. These results are in agreement with other studies that found lower tensile strengths, percentage elongations, and Young's moduli for films based on lower-molecular-weight chitosan in comparison to films based on higher-molecular-weight chitosan.[29,31] Refer to Table S1 for the numerical values (mean ± standard deviation) of the results.

3.5. Tissue Bonding Strength. Figure 4 summarizes the changes in the tissue bonding strength of chitosan−rose bengal films when modified with oligomeric chitosan, processed with freeze-drying, and irradiated with a green light. For all irradiated adhesive films, incorporating oligomeric chitosan at 10% did not significantly affect ($p > 0.05$) the tissue bonding strength when compared to films made from the standard composition, whereas adding oligomeric chitosan at 30% decreased the tissue bonding strength by ∼10% ($p < 0.0001$, one-way ANOVA, Tukey's post-test). There was no significant difference between the tissue bonding strengths of the porous and nonporous oligomeric 10% adhesives when irradiated (14.0 ± 1.1 vs 14.5 ± 1.2 kPa, n = 30, $p > 0.05$, one-way ANOVA, Tukey's post-test). However, the porous adhesives with the standard and oligomeric 30% compositions achieved ∼10% lower bonding strengths than the nonporous adhesives with the same compositions when irradiated ($p < 0.05$, one-way ANOVA, Tukey's post-test).

When the adhesive films were not irradiated, there was a sharp decrease in bonding strength in all groups as photo-

DOI: 10.1021/acsami.9b09123
ACS Appl. Mater. Interfaces 2019, 11, 32613−32622

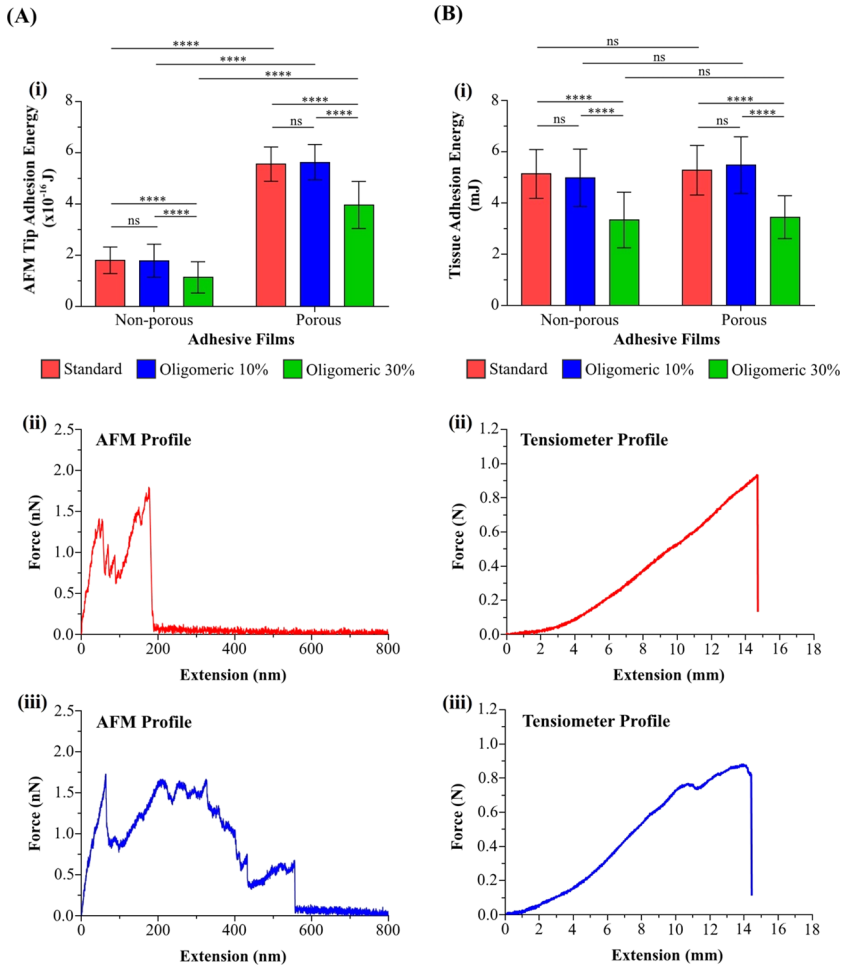

Figure 6. Plot (A-i) illustrates the energy required to detach the silicon tip of the AFM cantilever from the surface of different adhesive films; the adhesion toughness of the porous films was greater than that of the nonporous films. (A-ii) and (A-iii) show typical AFM force vs extension curves for a nonporous film (standard) and a porous film (oligomeric 10%), respectively; adhesion energy is the area under the curves, and the peaks represent the rupturing of polymer chains tethered to the tip as it moves up and away from the film surface. Plot (B-i) represents the tissue adhesion energy of different adhesives photochemically bonded to sheep small intestine tissue; the nonporous and porous adhesives have similar tissue adhesion energies. (B-ii) and (B-iii) show typical tensiometer force vs extension curves of tissue repaired with a nonporous film (standard) and a porous film (oligomeric 10%), respectively. In both tests (A, B), the films became less tough when oligomeric chitosan was incorporated at 30%. Data are displayed as mean ± standard deviation where $n = 54$ for (A-i) and $n = 30$ for (B-i). p values were determined by one-way ANOVA, Tukey's post-test, where **** signifies $p < 0.0001$ and ns signifies $p > 0.05$.

chemical reactions did not occur at the tissue interface. Interestingly, the tissue bonding strengths of the porous adhesives without irradiation were 3−5 times higher than those of the nonporous adhesives. It may be speculated that the porosity of the adhesive enhances tissue interlocking, leading to higher bonding strength (Figure 5). Cohesive failure (film breakage) occurred for all of the oligomeric 30% films and one-fifth of the irradiated porous oligomeric 10% films, while the remaining samples failed at the adhesive−tissue interface where the adhesive detached from the tissue surface.

These results indicate that the porous films can maintain strong adhesion on tissue without sutures. Fixing porous scaffolds with sutures is problematic because sutures can cause pain and obstruct blood flow at the surgical site.[32,33] Sutures may also place unnecessary tension on the scaffold, which can lead to tears in the material.

3.6. Adhesion Energy. Adhesion energy was measured to assess the ability of the films to accommodate deformations when bonded to surfaces. When examined on the nanoscale (Figure 6A), the energy needed to remove a nanosized AFM silicon tip from the surface of the porous films was approximately triple the energy required to remove the tip from the nonporous films with the same composition ($p < 0.0001$, one-way ANOVA, Tukey's post-test). On the macro-scale (Figure 6B), the energy required to remove the porous films photochemically bonded to the tissue was not significantly different from that required for the nonporous films with the same composition ($p > 0.05$, one-way ANOVA, Tukey's post-test). These results indicate that the porous films have a greater adhesion toughness; the films produce an adhesive bond that is more tolerant to immediate failure and allows for mechanical manipulation.

However, when oligomeric chitosan was added at 30%, the film's adhesion energy measured by both the AFM and tensiometer decreased by ∼30% when compared to that of the films of standard composition ($p < 0.0001$, one-way ANOVA, Tukey's post-test). The adhesion energies measured in both experiments for films with oligomeric 10% composition were not significantly different from those of the films made from the standard composition ($p > 0.05$, one-way ANOVA,

DOI: 10.1021/acsami.9b09123
ACS Appl. Mater. Interfaces 2019, 11, 32613−32622

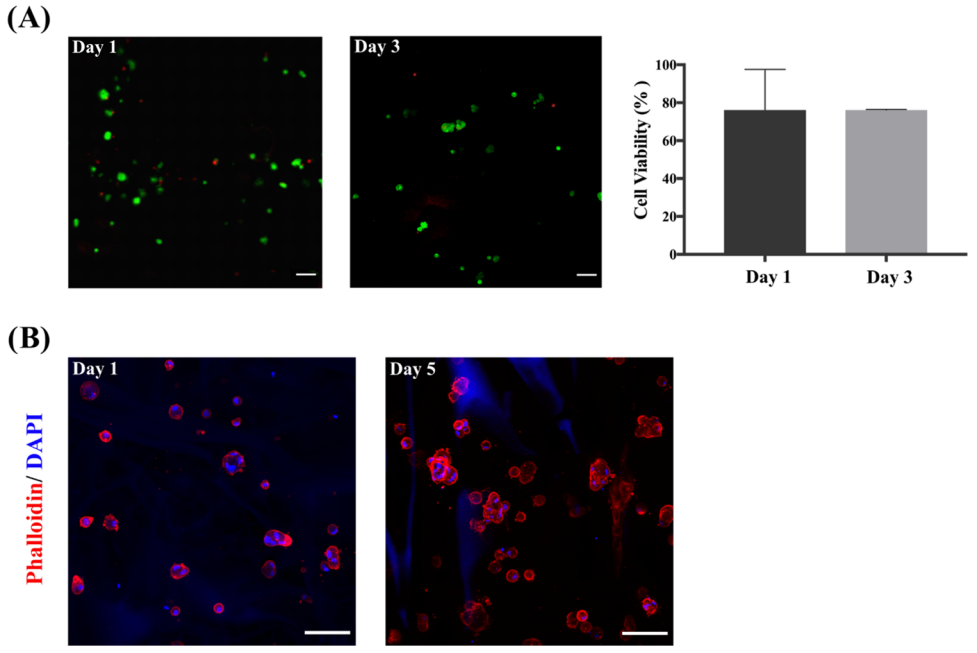

Figure 7. Live/dead imaging and hMSC morphology assessment. (A) shows cell viability and representative live (green)/dead (red) staining cells at day 1 and day 3 after initial culture within the porous oligomeric 10% films and a graph of live cell percentage at the two time points (live: p = 0.2097, paired t-test, n = 6−2; dead: p = 0.5277, paired t-test, n = 6−2). (B) shows immunofluorescence images of the hMSCs within the chitosan film. Cell morphology was assessed by rhodamine phalloidin (red) and DAPI (blue) staining after 1 day and 5 days. Scale bar = 100 μm. Blue autofluorescence of chitosan was observed in some samples without affecting quantitative analysis.

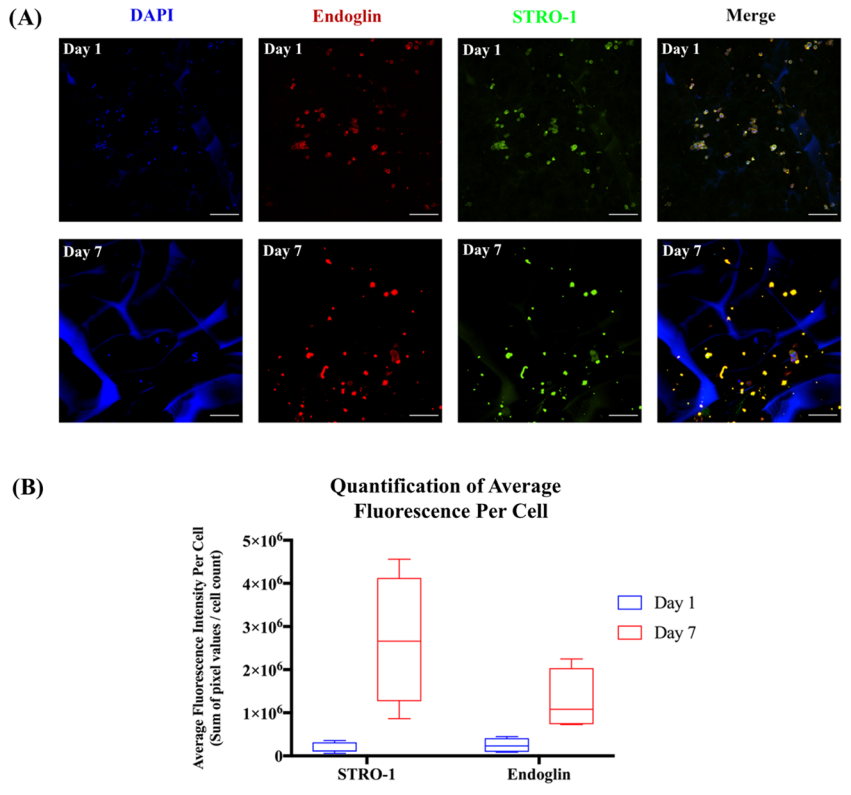

Figure 8. Immunofluorescence analysis of hMSC markers. Cells cultured on porous oligomeric 10% films were analyzed for the expression of endoglin (red) and STRO-1 (green) as shown in (A); nuclear staining with DAPI (blue). Quantification of average fluorescence per cell is shown in (B). There was a significant increase in the expression of STRO-1 and endoglin between days 1 and 7 (STRO-1: p = 0.0013, multiple t-tests, n = 7−4; endoglin: p = 0.0039, multiple t-tests, n = 7−4). For images in (A) day 1, scale bar = 200 μm, and for images in (A) day 7, scale bar = 100 μm. Blue autofluorescence of chitosan was observed in some samples without affecting quantitative analysis.

Tukey's post-test). The lower adhesion energy of the oligomeric 30% film was measured to be lower likely due to the film's brittleness (Figure 3) given that, in all of the tissue repair tests, these films failed cohesively before detaching from

DOI: 10.1021/acsami.9b09123
ACS Appl. Mater. Interfaces 2019, 11, 32613−32622

the tissue surface. Similarly, for the AFM measurements, the polymer chains of the oligomeric 30% films that were tethered to the AFM tip may have broken before detaching from the AFM tip.

3.7. Cell Viability and Activity. The porous oligomeric 10% films were selected for the in vitro cell study because they showed ideal properties for in vivo application: ∼20% of material dissolution can occur within 7 days (Figure 2A) while exhibiting tissue bonding strengths close to those of nonporous standard adhesives (Figure 4A). The viability of hMSCs was not significantly affected when cultured in these films where viabilities of 76.14 ± 10.78 and 76.03 ± 30.40% on days 1 and 3 were recorded, respectively (see Figure 7A). hMSCs maintained a uniform shape without evidence of protrusion or spreading, consistent with a low adhesive phenotype (Figure 7B), where control samples of hMSCs on glass coverslips showed considerable spreading and elongation (Figure S2). Additionally, hMSCs cultured in the films showed significantly increased expression of the hMSCS markers, STRO-1 (CD34) and endoglin (CD105), between day 1 (Figure 8A, top) and day 7 (Figure 8A, bottom) compared to the control cultures on glass coverslips (Figure S2). Cytoplasmic active STRO-1 expression increased almost 15-fold at day 7 of culturing with an intensity of $(26.90 \pm 15.10) \times 10^5$ compared to $(1.85 \pm 1.16) \times 10^5$ on day 1, while endoglin increased more than 5-fold during the same time frame $[(2.53 \pm 1.43) \times 10^5$ vs $(12.90 \pm 7.13) \times 10^5]$ (Figure 8B). We note that the chitosan material displayed variable degrees of autofluorescence from sample to sample in the blue channel; however, this did not impede quantification of molecular markers via immunofluorescence.

STRO-1 and endoglin have served as markers for multipotency in hMSCs and have also delineated populations with enhanced activity for neovascularization.[34] Our previous studies demonstrated increased expression of these markers in hMSCs when cultured under conditions of low cytoskeletal tension.[35] The increase in expression of STRO-1 and endoglin for the rounded hMSCs with low cytoskeletal tension in the chitosan films is consistent with this earlier report. Collectively, these results demonstrate the effectiveness of these chitosan films as a support for human stem cells for prolonged culture and further suggest that the architecture of the films can augment a phenotype, which may be useful for coronary artery disease treatment. For instance, we recently demonstrated how hMSCs with high endoglin expression display an angiogenic secretome, which can enhance neovascularization.[22]

The chitosan-based films may prove to be a more favorable stem cell delivery material compared to cell-derived ECMs for clinical translation. Cell-derived ECMs such as Matrigel and Cultrex (typically derived from mouse sarcoma cells) have several issues including batch-to-batch variability, inconsistent biophysical matrix, and uncharacterized protein compositions.[36] In addition to these production issues, cell-derived ECMs have a high cost, which impedes the scalability of most experiments.

It should be noted that the films were tested without rose bengal, as explained in Section 2.9.1. Several studies have shown that the level of reactive oxygen species produced by rose bengal when used for PTB does not have a significant effect on the growth and morphology of human fibroblasts in vitro and in vivo.[9,10,13,16,17,37] One study also noted that PTB using rose bengal does not have a detrimental effect on the growth of stem cells in vivo.[38]

4. CONCLUSIONS

This study demonstrated that porous chitosan-based adhesive films obtained through freeze-drying can form adhesive bonds to tissue with adequate strength and toughness without sutures when exposed to a green LED light. The porous films can support hMSC viability in vitro, where the hMSCs showed a rounded morphology with minimal spreading within the material, which corresponds to enhancement of the markers STRO-1 and endoglin after several days in culture. Adjusting the portion of oligomeric chitosan in the films can further tune the porosity, stiffness, swelling, and degradability, thereby opening up avenues for tailored sutureless scaffolds to support ECM synthesis and cell engraftment after dissolution for regenerative medicine.

■ ASSOCIATED CONTENT

Supporting Information

The Supporting Information is available free of charge on the ACS Publications website at DOI: 10.1021/acsami.9b09123.

Images of the adhesive films (Figure S1); table summarizing the adhesive properties (Table S1); immunofluorescence images of hMSCs cultured on a glass coverslip (Figure S2)

■ AUTHOR INFORMATION

Corresponding Author

*E-mail: A.lauto@westernsydney.edu.au.

ORCID

Damia Mawad: 0000-0002-6965-3232

Antonio Lauto: 0000-0003-4593-5603

Author Contributions

The study was planned and supervised by A.L. with the help of H.R., D.M., S.M., and K.K. The experiments on adhesion, swelling, erodibility, mechanical testing, and AFM characterization of the adhesives were performed by H.R. with the help of D.M., D.T., J.H., and A.L. R.W., L.G., and H.R. completed the SEM experiments. The stem cell study was done by S.R., J.I., and K.K. with the help of H.R., D.M., S.M., and A.L. Data analysis was done by A.L., H.R., and J.H. All Authors contributed to the writing of the manuscript.

Notes

The authors declare no competing financial interest.

■ ACKNOWLEDGMENTS

This work was supported by the School of Science and Health and the School of Medicine at the Western Sydney University, and the Department of Chemistry and Department of Materials Science and Engineering, at the University of New South Wales. The authors also acknowledge the support from the Advanced Materials Characterisation Facility at Western Sydney University, for the SEM work, and the Biomedical Imaging Facility at University of New South Wales, for the confocal microscopy work.

■ REFERENCES

(1) Alarcon, E. I.; Poblete, H.; Roh, H.; Couture, J.-F.; Comer, J.; Kochevar, I. E. Rose Bengal Binding to Collagen and Tissue Photobonding. *ACS Omega* **2017**, *2*, 6646−6657.

(2) Tsao, S.; Yao, M.; Tsao, H.; Henry, F. P.; Zhao, Y.; Kochevar, J. J.; Redmond, R. W.; Kochevar, I. E. Light-Activated Tissue Bonding

for Excisional Wound Closure: A Split-Lesion Clinical Trial. *Br. J. Dermatol.* **2012**, *166*, 555−563.
(3) Alejandre-Alba, N.; Gutierrez-Contreras, R.; Dorronsoro, C.; Marcos, S. Intraocular Photobonding to Enable Accommodating Intraocular Lens Function. *Transl. Vision Sci. Technol.* **2018**, *7*, No. 27.
(4) O'Neill, A. C.; Winograd, J. M.; Zeballos, J. L.; Johnson, T. S.; Randolph, M. A.; Bujold, K. E.; Kochevar, I. E.; Redmond, R. W. Microvascular Anastomosis Using a Photochemical Tissue Bonding Technique. *Lasers Surg. Med.* **2007**, *39*, 716−722.
(5) Franco, R. A.; Dowdall, J. R.; Bujold, K.; Amann, C.; Faquin, W.; Redmond, R. W.; Kochevar, I. E. Photochemical Repair of Vocal Fold Microflap Defects. *Laryngoscope* **2011**, *121*, 1244−1251.
(6) Ni, T.; Senthil-Kumar, P.; Dubbin, K.; Aznar-Cervantes, S. D.; Datta, N.; Randolph, M. A.; Cenis, J. L.; Rutledge, G. C.; Kochevar, I. E.; Redmond, R. W. A Photoactivated Nanofiber Graft Material for Augmented Achilles Tendon Repair. *Lasers Surg. Med.* **2012**, *44*, 645−652.
(7) Fairbairn, N. G.; Ng-Glazier, J.; Meppelink, A. M.; Randolph, M. A.; Valerio, I. L.; Fleming, M. E.; Winograd, J. M.; Redmond, R. W. Light-Activated Sealing of Nerve Graft Coaptation Sites Improves Outcome Following Large Gap Peripheral Nerve Injury. *Plast. Reconstr. Surg.* **2015**, *136*, 739−750.
(8) Lauto, A.; Ruprai, H.; Hook, J. M. In *Concise Encyclopedia of Biomedical Polymers and Polymeric Biomaterials*, 1st ed.; Mishra, M., Ed.; Taylor & Francis, 2017; pp 1−18.
(9) Barton, M. J.; Morley, J. W.; Stoodley, M. A.; Shaikh, S.; Mahns, D. A.; Lauto, A. Long Term Recovery of Median Nerve Repair Using Laser-Activated Chitosan Adhesive Films. *J. Biophotonics* **2015**, *8*, 196−207.
(10) Barton, M.; Morley, J. W.; Stoodley, M. A.; Ng, K. S.; Piller, S. C.; Duong, H.; Mawad, D.; Mahns, D. A.; Lauto, A. Laser-Activated Adhesive Films for Sutureless Median Nerve Anastomosis. *J. Biophotonics* **2013**, *6*, 938−949.
(11) Bhatt, N. K.; Khan, T. R.; Mejias, C.; Paniello, R. C. Nerve Transection Repair Using Laser-Activated Chitosan in a Rat Model. *Laryngoscope* **2017**, *127*, E253−E257.
(12) Frost, S. J.; Mawad, D.; Higgins, M. J.; Ruprai, H.; Kuchel, R.; Tilley, R. D.; Myers, S.; Hook, J. M.; Lauto, A. Gecko-Inspired Chitosan Adhesive for Tissue Repair. *NPG Asia Mater.* **2016**, *8*, No. e280.
(13) Barton, M.; Piller, S. C.; Mahns, D. A.; Morley, J. W.; Mawad, D.; Longo, L.; Lauto, A. In Vitro Cell Compatibility Study of Rose Bengal-Chitosan Adhesives. *Lasers Surg. Med.* **2012**, *44*, 762−768.
(14) Mawad, D.; Warren, C.; Barton, M.; Mahns, D.; Morley, J.; Pham, B. T. T.; Pham, N. T. H.; Kueh, S.; Lauto, A. Lysozyme Depolymerization of Photo-Activated Chitosan Adhesive Films. *Carbohydr. Polym.* **2015**, *121*, 56−63.
(15) Lauto, A.; Stoodley, M.; Barton, M.; Morley, J. W.; Mahns, D. A.; Longo, L.; Mawad, D. Fabrication and Application of Rose Bengal-Chitosan Films in Laser Tissue Repair. *J. Visualized Exp.* **2012**, No. e4158.
(16) Mawad, D.; Mansfield, C.; Lauto, A.; Perbellini, F.; Nelson, G. W.; Tonkin, J.; Bello, S. O.; Carrad, D. J.; Micolich, A. P.; Mahat, M. M.; Furman, J.; Payne, D.; Lyon, A. R.; Gooding, J. J.; Harding, S. E.; Terracciano, C. M.; Stevens, M. M. A Conducting Polymer with Enhanced Electronic Stability Applied in Cardiac Models. *Sci. Adv.* **2016**, *2*, No. e1601007.
(17) Lauto, A.; Mawad, D.; Barton, M.; Gupta, A.; Piller, S. C.; Hook, J. Photochemical Tissue Bonding with Chitosan Adhesive Films. *Biomed. Eng. Online* **2010**, *9*, 47−57.
(18) Verter, E. E.; Gisel, T. E.; Yang, P.; Johnson, A. J.; Redmond, R. W.; Kochevar, I. E. Light-Initiated Bonding of Amniotic Membrane to Cornea. *Invest. Ophthalmol. Visual Sci.* **2011**, *52*, 9470−9477.
(19) Fereshteh, Z. Freeze-Drying Technologies for 3D Scaffold Engineering. In *Functional 3D Tissue Engineering Scaffolds: Materials, Technologies and Applications*; Deng, Y., Kuiper, J., Eds.; Woodhead Publishing: U.K., 2018; pp 151−174.
(20) Wang, X.; Rivera-Bolanos, N.; Jiang, B.; Ameer, G. A. Advanced Functional Biomaterials for Stem Cell Delivery in Regenerative Engineering and Medicine. *Adv. Funct. Mater.* **2019**, *29*, No. 1809009.
(21) Mayourian, J.; Cashman, T. J.; Ceholski, D. K.; Johnson, B. V.; Sachs, D.; Kaji, D. A.; Sahoo, S.; Hare, J. M.; Hajjar, R. J.; Sobie, E. A.; Costa, K. D. Experimental and Computational Insight into Human Mesenchymal Stem Cell Paracrine Signaling and Heterocellular Coupling Effects on Cardiac Contractility and Arrhythmogenicity. *Circ. Res.* **2017**, *121*, 411−423.
(22) Abdeen, A. A.; Weiss, J. B.; Lee, J.; Kilian, K. A. Matrix Composition and Mechanics Direct Proangiogenic Signaling from Mesenchymal Stem Cells. *Tissue Eng., Part A* **2014**, *20*, 2737−2745.
(23) Bagno, L.; Hatzistergos, K. E.; Balkan, W.; Hare, J. M. Mesenchymal Stem Cell-Based Therapy for Cardiovascular Disease: Progress and Challenges. *Mol. Ther.* **2018**, *26*, 1610−1623.
(24) Miller-Chou, B. A.; Koenig, J. L. A Review of Polymer Dissolution. *Prog. Polym. Sci.* **2003**, *28*, 1223−1270.
(25) Ouyang, Q.; Ishida, K.; Okada, K. Investigation of Micro-Adhesion by Atomic Force Microscopy. *Appl. Surf. Sci.* **2001**, *169−170*, 644−648.
(26) Yaghobi, N. Controlling Chitosan's Molecular Weight Via Multistage Deacetylation. *Biotechnol. Bioprocess Eng.* **2012**, *17*, 812−817.
(27) Tian, M.; Tan, H.; Li, H.; You, C. Molecular Weight Dependence of Structure and Properties of Chitosan Oligomers. *RSC Adv.* **2015**, *5*, 69445−69452.
(28) Ruiz-Caro, R.; Veiga-Ochoa, M. D. Characterization and Dissolution Study of Chitosan Freeze-Dried Systems for Drug Controlled Release. *Molecules* **2009**, *14*, 4370−4386.
(29) Barton, M. J.; Morley, J. W.; Mahns, D. A.; Mawad, D.; Wuhrer, R.; Fania, D.; Frost, S. J.; Loebbe, C.; Lauto, A. Tissue Repair Strength Using Chitosan Adhesives with Different Physical-Chemical Characteristics. *J. Biophotonics* **2014**, *7*, 948−955.
(30) Handorf, A. M.; Zhou, Y.; Halanski, M. A.; Li, W.-J. Tissue Stiffness Dictates Development, Homeostasis, and Disease Progression. *Organogenesis* **2015**, *11*, 1−15.
(31) Nunthanid, J.; Puttipipatkhachorn, S.; Yamamoto, K.; Peck, G. E. Physical Properties and Molecular Behavior of Chitosan Films. *Drug Dev. Ind. Pharm.* **2001**, *27*, 143−157.
(32) Carbonell, A. M.; Harold, K. L.; Mahmutovic, A. J.; Hassan, R.; Matthews, B. D.; Kercher, K. W.; Sing, R. F.; Heniford, B. T. Local Injection for the Treatment of Suture Site Pain after Laparoscopic Ventral Hernia Repair. *Am. Surg.* **2003**, *69*, 688−691 discussion 691−682 .
(33) Schlechter, B.; Guyuron, B. A Comparison of Different Suture Techniques for Microvascular Anastomosis. *Ann. Plast. Surg.* **1994**, *33*, 28−31.
(34) Mangialardi, G.; Cordaro, A.; Madeddu, P. The Bone Marrow Pericyte: An Orchestrator of Vascular Niche. *Regener. Med.* **2016**, *11*, 883−895.
(35) Zhang, D.; Kilian, K. A. The Effect of Mesenchymal Stem Cell Shape on the Maintenance of Multipotency. *Biomaterials* **2013**, *34*, 3962−3969.
(36) Hughes, C. S.; Postovit, L. M.; Lajoie, G. A. Matrigel: A Complex Protein Mixture Required for Optimal Growth of Cell Culture. *Proteomics* **2010**, *10*, 1886−1890.
(37) Yao, M.; Gu, C.; Doyle, F. J., Jr.; Zhu, H.; Redmond, R. W.; Kochevar, I. E. Why Is Rose Bengal More Phototoxic to Fibroblasts in Vitro Than in Vivo? *Photochem. Photobiol.* **2014**, *90*, 297−305.
(38) Gu, C.; Ni, T.; Verter, E. E.; Redmond, R. W.; Kochevar, I. E.; Yao, M. Photochemical Tissue Bonding: A Potential Strategy for Treating Limbal Stem Cell Deficiency. *Lasers Surg. Med.* **2011**, *43*, 433−442.

DOI: 10.1021/acsami.9b09123
ACS Appl. Mater. Interfaces 2019, 11, 32613−32622